Contribution from the Departments of Chemistry, University of Utah, Salt Lake City, Utah 84112, and University of Delaware, Newark, Delaware 19716, Department of Chemistry and Materials Science Center, Cornell University, Ithaca, New York 14853-1301, and Fachbereich 6-Anorganische Chemie-der Universität-GH Duisburg, Lotharstrasse 1, D-4100 Duisburg 1, FRG

Structure and Bonding in Cationic Cyclopentadienyliron Complexes Containing Thio-, Seleno-, and Telluroethers as Ligands[1]

Hans Schumann,*[,†,2] Atta M. Arif,*[,†] Arnold L. Rheingold,*[,‡] Christoph Janiak,[§] Roald Hoffmann,*[,§] and Norbert Kuhn[∥]

Received August 3, 1990

An extended Hückel MO study based on X-ray structure determinations of $[C_5H_5Fe(CO)_2(ER_2)]BF_4$ complexes (I: E = S, R = CH_3, C_6H_5; E = Se, Te, R = CH_3) and their chemistry confirms and rationalizes the inertness and stability of the Fe–E bond in these cations in the order E = Te ≫ Se > S > O on the basis of electronegativity, orbital diffuseness, and size considerations. No important π-bonding effect is found, and a comment on the photochemical replacement of CO is made. The different lability trend for the related $[C_5H_5Fe(CO)_2(E'R_3)]^+$ cations (II: E' = N–Bi, R = CH_3) is compared and briefly discussed on the basis of extended Hückel MO calculations. The complexes $[C_5H_5Fe(CO)_2(E(CH_3)_2)]BF_4$ crystallize in the monoclinic space group $P2_1/n$ (E = S) or $P2_1/c$ (E = Se, Te) with the unit cell parameters (in the order S, Se, and Te) a = 8.133 (2), 8.256 (3), 8.393 (2) Å, b = 12.801 (5), 12.798 (5), 12.890 (5) Å, c = 13.269 (2), 13.404 (5), 13.411 (7) Å, β = 106.89 (1), 109.21 (3), 109.46 (3)°, and Z = 4. The complex $[C_5H_5Fe(CO)_2(S(C_6H_5)_2)]BF_4$ crystallizes in the orthorhombic space group *Pbca* with the unit cell parameters a = 9.783 (2) Å, b = 19.452 (5) Å, c = 20.554 (6) Å, and Z = 8. All complexes show a three-legged piano-stool geometry around the iron center with Fe–E distances of 2.264 (2) and 2.283 (4) Å (E = S, R = CH_3 and C_6H_5), 2.381 (1) Å (E = Se), and 2.533 (1) Å (E = Te).

Introduction

In previous papers on the coordination chemistry of $E(CH_3)_n$ ligands containing group 15 (n = 3, E = N–Bi)[3] or group 16 (n = 2, E = O–Te)[4] donor elements E, we discussed the coordination properties of these ligands on the basis of spectroscopic data and ligand displacement reactions, as well as their photochemical reactivity: in $[C_5H_5Fe(CO)_2(ER_2)]^+$ cations Ia–C (E = S, Se, Te, R = CH_3), the heavier E ligands replace their lighter congeners under thermal conditions. That means E = S, Se, and Te readily replace OR_2 ligands; E = Te replaces S and Se ligands irreversibly, while Se versus S forms an equilibrium which lies, however, on the Se side. Under thermal conditions, O, S, and Se ligands are also substituted by phosphine (PR_3) ligands, but not TeR_2. An increasing electron density on the metal center is observed in the order Fe–O < Fe–S < Fe–Se < Fe–Te.[4a] Photochemical conditions lead to the replacement of a CO group in Ia–c by another ligand L (L = $E(CH_3)_2$ or PR_3) to give $[C_5H_5Fe(CO)(E(CH_3)_2)L]^+$.[4b] The above properties and trends were noted to be different from group 15 ligands $E'R_3$ (E' = N–Bi), where BiR_3 ligands are the most weakly coordinated ones in $[C_5H_5Fe(CO)_2]^+$ complexes. Ligand-exchange experiments using uncoordinated $E'(CH_3)_3$ established the order of displacement ability as P ≫ As > Sb > N > Bi.[3a,3c] On the basis of these studies, bond strengths for the Fe–$E(CH_3)_n$ bond were suggested to decrease for group 15 elements in the order E' = P > As > Sb > N > Bi and for group 16 elements in the order E = Te ≫ Se > S ≫ O. With respect to the trends in the well-investigated group 15 donor ligand series, the surprising observation of the ligand $Te(CH_3)_2$ as the ligand most strongly bonded to the iron fragment was explained by a possible additional interaction between the iron center and the second lone pair on Te.[4a] Concerning the comparative ease for the displacement of the ER_2 ligands from complexes I, the term *bond strength* was used in our earlier publications.[3,4] When the substitution of ER_2 ligands by phosphines or related strong ligands was discussed, the Fe–Te bond was said to be extremely *stable*. However, while the Fe–Te bond may be *stronger* or more *stable* than the Fe–S bond in cationic complexes, we think it is important here that it is more *inert* to substitution. Instead of discussing the above results from a *thermodynamic* point of view, using the terms *stable* and *unstable*, we feel a discussion from the *kinetic* viewpoint in terms of *labile* or *inert* is more appropriate.

To gain further insight in the bonding situation of group 16 $E(CH_3)_2$ ligands, the structures of four $[C_5H_5Fe(CO)_2(ER_2)]^+$ complexes were determined by X-ray diffraction and the obtained geometries were used for extended Hückel MO calculations on the model cations $[C_5H_5Fe(CO)_2(EH_2)]^+$ (E = S–Te). This paper describes the first comprehensive molecular structure study on complexes with $E(CH_3)_2$ ligands together with conclusions for the bonding and chemistry of these ligands as obtained by extended Hückel MO calculations.

Experimental Section

X-ray Structure Determinations (Table I). All compounds used in this study were prepared as described in the literature.[5] Crystals suitable for X-ray diffraction studies were obtained by slow diffusion of a pentane/ether mixture (1/2) into dilute methylene chloride/acetone solutions of complexes Ia–d at room temperature in the dark over 1–3 days. The crystals were obtained as yellow to orange air-stable blocks and mounted on either a Syntex $P\bar{1}$ (University of Utah, complexes Ia and Id) or a Nicolet R3m/μ diffractometer (University of Delaware, complexes Ib and Ic). Unit cell dimensions (Table I) were determined by least-squares refinement of the best angular positions for 15/25 (Utah/Delaware) independent reflections ($2\theta > 20°$) during normal alignment procedures using molybdenum radiation (λ = 0.710 73 Å). The data were collected at 289 K (complexes Ia and Id) and at 296 K (Ib and Ic) with a variable scan rate, θ–2θ mode, and a scan width of 1° below $K\alpha_1$ and 1° above $K\alpha_2$. The 2θ limits for the data collections are 4–50° (Ia and Ic), 4–48° (Ib), and 3–42° (Id). Data collections for complexes Ia–d showed <1% variation of the standard reflections and were corrected for absorption and Lorentz effects. Structures were solved by direct methods as implemented in SDP-PLUS[6] or SHELXTL[7] program collections. Refinements of scale factor, positional, and anisotropic thermal parameters for all non-hydrogen atoms were carried out to convergence within these program collections. The observed high R/R_w values for complex Id were due to the low quality of the crystal.[8] Positional parameters are given in Tables II–V and important bond distances and angles in Tables VI (complexes Ia–c) and VII (complex Id).

† University of Utah.
‡ University of Delaware.
§ Cornell University.
∥ Universität GH Duisburg.

(1) Presented in part at the IVth European Symposium on Inorganic Chemistry, Freiburg, FRG, Sept 1988; Abstract D21.
(2) Present address: Bensberger Strasse 15a, D-5064 Rösrath, FRG.
(3) (a) Schumann, H. *Chem.-Ztg.* **1986**, *111*, 121. (b) Schumann, H.; Speis, M.; Bisman, W. P.; Smits, J. M. M.; Beurskens, P. T. *J. Organometal. Chem.*, in press. (c) Schumann, H.; Eguren, L. *J. Organomet. Chem.*, in press.
(4) (a) Kuhn, N.; Schumann, H. *J. Organomet. Chem.* **1984**, *276*, 55. (b) Kuhn, N.; Schumann, H.; Zauder, E. *J. Organomet. Chem.* **1987**, *327*, 17. (c) Kuhn, N.; Schumann, H.; Winter, M.; Zauder, E. *Chem. Ber.* **1988**, *121*, 111.
(5) Schumann, H. *J. Organomet. Chem.* **1986**, *304*, 341.
(6) SDP-PLUS Program Package. Enraf-Nonius, The Netherlands, 1985.
(7) Sheldrick, G. SHELXTL Program Package. Nicolet XRD, Madison, WI, 1976.
(8) Only the Fe–S bond distance will be used for further discussion.

0020-1669/91/1330-1618$02.50/0

Table I. Crystallographic and Data Collection Parameters

formula	$C_9H_{11}BF_4FeO_2S$	$C_9H_{11}BF_4FeO_2Se$	$C_9H_{11}BF_4FeO_2Te$	$C_{19}H_{15}BF_4FeO_2S$
complex	Ia	Ib	Ic	Id
mol wt	325.9	372.8	421.4	450.1
cryst syst	monoclinic	monoclinic	monoclinic	orthorhombic
space group	$P2_1/n$	$P2_1/c$	$P2_1/c$	*Pbca*
a, Å	8.133 (2)	8.256 (3)	8.393 (2)	9.783 (2)
b, Å	12.801 (5)	12.798 (5)	12.890 (5)	19.452 (5)
c, Å	13.269 (2)	13.404 (5)	13.411 (7)	20.554 (6)
β, deg	106.89 (1)	109.21 (3)	109.46 (3)	
V, Å^3	1328	1337.5 (9)	1367.8 (1)	3911.6
μ(Mo Kα), cm^{-1}	13.26	40.9	33.0	9.19
D_c, g cm^{-3}	1.64	1.85	2.05	1.53
Z	4	4	4	8
obsd reflcns	1604	1661	1971	786
R/R_w[a]	5.66/5.59	4.93/5.81	3.11/3.92	11.53/13.12
GOF	1.85	1.36	1.41	4.66
CD,[b] mm	0.40 × 0.32 × 0.30	0.25 × 0.27 × 0.32	0.21 × 0.21 × 0.31	0.38 × 0.25 × 0.18

[a] $R = \sum(|F_o| - |F_c|)/\sum|F_o|$ and $R_w = |\sum w|F_o| - |F_c|^2/w(F_o)^2]^{1/2}$. [b] CD = crystal dimensions.

Table II. Positional Parameters for $[C_5H_5Fe(CO)_2(S(CH_3)_2)]BF_4$ (Ia)

atom	*x* ($\sigma(x)$)	*y* ($\sigma(y)$)	*z* ($\sigma(z)$)
Fe	0.5624 (1)	0.06716 (8)	0.77233 (7)
S	0.3524 (2)	0.1153 (2)	0.6264 (1)
F1	0.1385 (7)	−0.2849 (5)	0.4939 (5)
F2	0.4162 (7)	−0.2721 (7)	0.5182 (5)
F3	0.3203 (8)	−0.2654 (6)	0.6511 (4)
F4	0.272 (1)	−0.1390 (5)	0.5407 (6)
O1	0.3339 (6)	−0.0094 (5)	0.8900 (4)
O2	0.6090 (8)	0.2754 (4)	0.8647 (4)
C1	0.4205 (8)	0.0239 (6)	0.8438 (5)
C2	0.5867 (8)	0.1958 (6)	0.8284 (5)
C3	0.659 (1)	−0.08313 (7)	0.7684 (8)
C4	0.656 (1)	−0.0331 (9)	0.6767 (6)
C5	0.7532 (9)	0.0533 (8)	0.6995 (7)
C6	0.8267 (9)	0.0538 (9)	0.8071 (9)
C7	0.763 (1)	−0.0287 (8)	0.8510 (7)
C8	0.1489 (9)	0.0701 (9)	0.6348 (7)
C9	0.316 (1)	0.2536 (7)	0.6286 (7)
B	0.285 (1)	−0.2414 (7)	0.5521 (6)

Table III. Positional Parameters for $[C_5H_5Fe(CO)_2(Se(CH_3)_2)]BF_4$ (Ib)

atom	*x* ($\sigma(x)$)	*y* ($\sigma(y)$)	*z* ($\sigma(z)$)
Fe	0.2880 (1)	0.07441 (8)	0.22260 (7)
Se	0.22832 (9)	0.11724 (6)	0.37984 (5)
F1	0.8193 (11)	0.2590 (7)	0.6518 (6)
F2	0.5925 (9)	0.2661 (7)	0.5126 (7)
F3	0.7482 (13)	0.1258 (4)	0.5388 (7)
F4	0.8492 (10)	0.2728 (6)	0.4937 (7)
O1	0.2359 (9)	0.2873 (5)	0.1393 (6)
O2	−0.0562 (7)	−0.0005 (5)	0.1069 (5)
C1	0.2540 (10)	0.2058 (7)	0.1716 (6)
C2	0.0751 (10)	0.0324 (5)	0.1532 (5)
C3	0.3894 (15)	−0.0747 (8)	0.2292 (12)
C4	0.3993 (14)	−0.0235 (11)	0.1390 (8)
C5	0.5025 (15)	0.0603 (10)	0.1774 (12)
C6	0.5511 (13)	0.06552 (14)	0.2844 (12)
C7	0.4833 (17)	−0.0193 (15)	0.3156 (8)
C8	0.1737 (15)	0.2638 (7)	0.3738 (8)
C9	−0.0037 (11)	0.0702 (10)	0.3610 (7)
B	0.7532 (13)	0.2328 (8)	0.5478 (8)

Extended Hückel MO Calculations. The computations were performed within the extended Hückel formalism[9] with weighted H_{ij}'s.[10] The atomic parameters for the elements involved in our calculations are given in Table VIII. The established literature parameter for the sulfur 3p valence state ionization potential is actually −11.0 eV.[11] However, using this literature value gives bad agreement in the Fe charge dependency,[12] although not in the Fe–E overlap population variation for S. Since a

Table IV. Positional Parameters for $[C_5H_5Fe(CO)_2(Te(CH_3)_2)]BF_4$ (Ic)

atom	*x* ($\sigma(x)$)	*y* ($\sigma(y)$)	*z* ($\sigma(z)$)
Fe	0.28953 (8)	0.07631 (5)	0.21549 (5)
Te	0.23341 (4)	0.11614 (2)	0.38572 (2)
F1	0.8011 (9)	0.2528 (6)	0.6479 (5)
F2	0.5903 (6)	0.2611 (5)	0.5028 (6)
F3	0.7426 (9)	0.1209 (3)	0.5385 (6)
F4	0.8450 (7)	0.2620 (5)	0.4955 (6)
O1	0.2377 (6)	0.2902 (4)	0.1434 (4)
O2	−0.0561 (5)	0.0101 (4)	0.1062 (3)
C1	0.2561 (7)	0.2067 (4)	0.1722 (4)
C2	0.0794 (6)	0.0387 (4)	0.1495 (4)
C3	0.3870 (12)	−0.0705 (6)	0.2161 (11)
C4	0.3949 (9)	−0.0180 (7)	0.1317 (5)
C5	0.4985 (11)	0.0653 (8)	0.1680 (9)
C6	0.5470 (8)	0.0624 (11)	0.2758 (10)
C7	0.4808 (18)	−0.0225 (14)	0.3007 (8)
C8	0.1656 (12)	0.2742 (5)	0.3741 (6)
C9	−0.0164 (7)	0.0661 (7)	0.3594 (5)
B	0.7460 (8)	0.2225 (5)	0.5492 (6)

Table V. Positional Parameters for $[C_5H_5Fe(CO)_2(S(C_6H_5)_2)]BF_4$ (Id)[a]

atom	*x* ($\sigma(x)$)	*y* ($\sigma(y)$)	*z* ($\sigma(z)$)
Fe	0.8341 (5)	0.1654 (3)	0.6134 (2)
S	0.7000 (8)	0.0702 (4)	0.6006 (4)
F1*	0.314 (4)	0.315 (2)	0.170 (2)
F2*	0.634 (3)	0.717 (1)	0.329 (1)
F3*	0.656 (4)	0.237 (2)	0.327 (2)
F4*	0.230 (5)	0.760 (2)	0.086 (2)
O1	0.999 (3)	0.106 (1)	0.716 (1)
O2	1.023 (3)	0.135 (1)	0.508 (1)
C1	0.925 (4)	0.129 (2)	0.677 (2)
C2	0.956 (4)	0.147 (2)	0.553 (2)
C3	0.845 (5)	0.255 (2)	0.667 (2)
C4	0.692 (4)	0.222 (2)	0.665 (2)
C5	0.659 (4)	0.225 (2)	0.601 (2)
C6	0.754 (4)	0.256 (2)	0.569 (2)
C7	0.859 (3)	0.271 (2)	0.604 (2)
C8	0.783 (4)	0.001 (2)	0.636 (2)
C9	0.698 (4)	−0.028 (2)	0.691 (2)
C10	0.772 (4)	−0.085 (2)	0.722 (2)
C11	0.899 (4)	−0.109 (2)	0.704 (2)
C12	0.963 (4)	−0.080 (2)	0.651 (2)
C13	0.895 (3)	−0.028 (2)	0.620 (2)
C14	0.694 (4)	0.043 (2)	0.519 (2)
C15	0.682 (4)	0.090 (2)	0.469 (2)
C16	0.665 (4)	0.070 (2)	0.403 (2)
C17	0.663 (4)	0.001 (2)	0.389 (2)
C18	0.675 (5)	−0.049 (2)	0.436 (2)
C19	0.678 (4)	−0.029 (2)	0.503 (2)
B*	0.721	0.764	0.360

[a] Starred atoms were refined isotropically.

(9) (a) Hoffmann, R. *J. Chem. Phys.* **1963**, *39*, 1397. (b) Hoffmann, R.; Lipscomb, W. N. *J. Chem. Phys.* **1962**, *36*, 2179. (c) Hoffmann, R.; Lipscomb, W. N. *J. Chem. Phys.* **1962**, *37*, 2872.
(10) Ammeter, J. H.; Bürgi, H.-B.; Thibeault, J. C.; Hoffmann, R. *J. Am. Chem. Soc.* **1978**, *100*, 3686.
(11) Chen, M. M. L.; Hoffmann, R. *J. Am. Chem. Soc.* **1976**, *98*, 1647.

Table VI. Selected Bond Distances (Å) and Angles (deg) for $[C_5H_5Fe(CO)_2(E(CH_3)_2)]BF_4$

	E = S (Ia)	E = Se (Ib)	E = Te (Ic)
Fe–E	2.264 (2)	2.381 (1)	2.533 (1)
Fe–C1	1.781 (8)	1.802 (9)	1.770 (5)
Fe–C2	1.794 (7)	1.780 (7)	1.757 (5)
Fe–C_5H_5(av)	2.072	2.068	2.057
E–C8	1.787 (9)	1.924 (9)	2.107 (7)
E–C9	1.797 (9)	1.943 (9)	2.108 (7)
O1–C1	1.14 (1)	1.211 (11)	1.135 (7)
O2–C2	1.119 (9)	1.138 (9)	1.152 (6)
E–Fe–C1	95.5 (2)	94.0 (3)	92.7 (2)
E–Fe–C2	94.0 (2)	94.3 (3)	93.1 (2)
Fe–C1–O1	176.0 (7)	178.5 (8)	178.4 (6)
Fe–C2–O2	177.1 (6)	175.3 (7)	177.3 (5)
Fe–E–C8	109.9 (3)	107.5 (4)	104.9 (2)
Fe–E–C9	110.0 (3)	107.2 (3)	105.1 (2)
C8–E–C9	99.0 (5)	95.1 (5)	93.1 (4)

Table VII. Selected Bond Distances (Å) and Angles (deg) for $[C_5H_5Fe(CO)_2(S(C_6H_5)_2)]BF_4$ (Id)

Fe–S	2.283 (4)	S–C8	1.74 (2)
Fe–C1	1.73 (1)	S–C14	1.76 (1)
Fe–C2	1.75 (2)	O1–C1	1.17 (2)
Fe–C_5H_5(av)	2.09	O2–C2	1.16 (2)
S–Fe–C1	92.9 (5)	Fe–S–C8	108.2 (6)
S–Fe–C2	98.5 (6)	Fe–S–C14	111.8 (5)
Fe–C1–O1	172 (1)	C8–S–C14	100.5 (8)
Fe–C2–O2	171 (2)		

Table VIII. Parameters Used in the Extended Hückel Calculations

atom	orbital	H_{ij}, eV	ζ_1[a]	ref
Fe	4s	−9.10	1.90	17
	4p	−5.32	1.90	
	3d	−12.60	5.35[b]	
O	2s	−32.3	2.275	9a
	2p	−14.8	2.275	
S	3s	−20.0	2.122	12[c]
	3p	−14.5	1.827	
Se	4s	−20.5	2.44	18
	4p	−14.4	2.07	
Te	5s	−20.78	2.51	19
	5p	−13.2	2.16	
N	2s	−26.0	1.95	9a
	2p	−13.2	1.95	
P	3s	−18.6	1.75	17
	3p	−14.0	1.30	
As	4s	−16.22	2.23	20
	4p	−12.16	1.89	
Sb	5s	−18.8	2.232	21
	5p	−11.7	1.999	
Bi	6s	−15.9	2.56	22
	6p	−7.79	2.07	
C	2s	−21.4	1.625	9a
	2p	−11.4	1.625	
H	1s	−13.6	1.3	9a

[a] Slater exponent. [b] ζ_2 = 2.00. Coefficients used in the double ζ expansion of the d orbitals: c_1 = 0.5505, c_2 = 0.6260. [c] Compare Experimental Section.

comparison of the atom parameters in Table VIII indicates that a value of −11.0 eV for S would be out of line in the *np* orbital energy series from O to Te, we felt justified in choosing a value of −14.5 eV. Geometrical parameters were fixed at some average value from the above molecular structures of Ia–c: Fe–$C_5H_{5center}$ = 172, C–C = 136, C–H = 108, Fe–C_{CO} = 180, C–O = 113, Fe–O = 195 (estimated),[13] Fe–S = 226, Fe–Se = 238, Fe–Te = 253, O–H = 96,[13] S–H = 134,[10] Se–H = 146,[13] Te–H = 170 pm;[13] $C_5H_{5center}$–Fe–C_{CO} = 125, $C_5H_{5center}$–Fe–E = 125, Fe–C–O = 180, Fe–E–H = 108, E–Fe–$C_5H_{5center}$–C_{CO} = ±120, $C_5H_{5center}$–Fe–E–H = ±132°. In the E′ complexes $[C_5H_5Fe(CO)_2(E'R_3)]^+$ (II: E′ = N–Bi), the same $[C_5H_5Fe(CO)_2]^+$ fragment geometry was employed as above. Other distances and angles were chosen: Fe–N = 185 (estimated), [13]Fe–P = 224,[14] Fe–As = 234,[15] Fe–Sb = 248,[16] Fe–Bi = 257,[3c] N–H = 101,[13] P–H = 142,[13] As–H = 152[13] Sb–H = 171,[13] Bi–H = 181 pm (estimated);[13] Fe–E′–H = 116, $C_5H_{5center}$–Fe–E′–H = 0, ±120°. Results of extended Hückel MO calculations are summarized in Tables IX–XI.

(12) The S 3p valence state ionization potential had to be adjusted to −14.5 eV compared to a literature value of −11.0 eV[11] in order to see the trend of increasing electron density on iron.

(13) (a) Ball, M. C.; Norbury, A. H. *Physical Data for Inorganic Chemists*; Longman: London, 1974; p 148. (b) Huheey, J. E. *Inorganic Chemistry*, 3rd ed.; Harper and Row; Cambridge, U.K., 1983; p A-32.

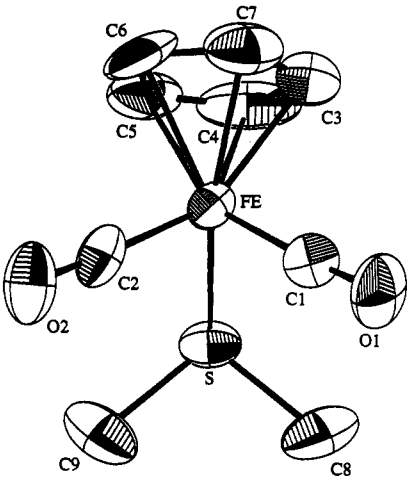

Figure 1. ORTEP diagram of the complex cation $[C_5H_5Fe(CO)_2(S(CH_3)_2)]^+$ (same numbering scheme for complexes Ia–c).

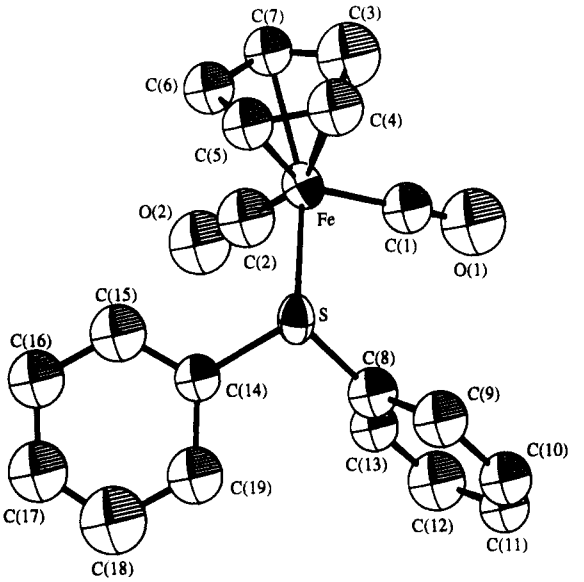

Figure 2. ORTEP diagram of the complex cation $[C_5H_5Fe(CO)_2(S(C_6H_5)_2)]^+$ (Id).

Results and Discussion

(A) Crystallographic Results. The complexes $[C_5H_5Fe(CO)_2(E(CH_3)_2)]^+$ (Ia–c; E = S, Se, Te) were found to be isomorphous, forming monoclinic crystals of the space group $P2_1/n$ or $P2_1/c$ with Z = 4. Least-squares refinement (Table I), as

(14) Sim, G. A.; Woodhouse, D. I.; Knox, G. R. *J. Chem. Soc., Dalton Trans.* **1979**, 629.
(15) Schumann, H.; Smits, J. M. M.; Beurskens, P. T. *J. Crystallogr. Spectrosc. Res.* **1989**, *19*, 1033.
(16) Cobbledick, R. E.; Einstein, F. W. B. *Acta Crystallogr.* **1978**, *B34*, 1473.
(17) Summerville, R. H.; Hoffmann, R. *J. Am. Chem. Soc.* **1976**, *98*, 7240.
(18) Gressier, P.; Whangbo, M.-H.; Meerschaut, A.; Rouxel, J. *Inorg. Chem.* **1984**, *23*, 1221.
(19) Canadell, E.; Mathey, Y.; Whangbo, M.-H. *J. Am. Chem. Soc.* **1988**, *110*, 104.
(20) Underwood, D. J.; Nowak, M.; Hoffmann, R. *J. Am. Chem. Soc.* **1984**, *106*, 2837.
(21) Hughbanks, T.; Hoffmann, R.; Whangbo, M.-H.; Stewart, K. R.; Eisenstein, O.; Canadell, E. *J. Am. Chem. Soc.* **1982**, *104*, 3876.
(22) Lohr, L. L.; Pyykkö, P. *Chem. Phys. Lett.* **1979**, *62*, 333.

Table IX. Summary of Various Calculated Parameters in the Analysis of $[C_5H_5Fe(CO)_2(EH_2)]^+$ and $[C_5H_5Fe(CO)_2(EH_3)]^{2+}$ Complexes

	overlap populations for Fe–E					$CpFe(CO)_2EH_3^{2+}$	
	filled levels	empty, low-lying, most antibonding orbital[a]	diff[b] $\lvert OP_{filled}\rvert - \lvert OH_{empty}\rvert$	dissocn energy,[c] eV	net charge on Fe	overlap pop. for Fe–E_{prot}	Δ(overlap pop.) (nonprotonated − protonated)[d]
O	0.235	−0.184 (LUMO)	0.051	0.489	0.0082	0.221	0.014
S	0.397	−0.113 (LUMO)	0.284	0.833	−0.168	0.410	−0.014
Se	0.403	−0.112 (LUMO)	0.291	0.969	−0.176	0.421	−0.018
Te	0.423	−0.077 (LUMO)	0.346	1.426	−0.249	0.450	−0.027

[a] Overlap populations for normally unoccupied orbitals were computed by filling them with two electrons each. [b] The difference is taken between the absolute values of the two Fe–E overlap populations. [c] Dissociation energy $= -[E_{complex} - E_{fragments}] = -[E_{complex} - (E_{CpFe(CO)_2^+} + E_{E(element)H_2}]$, E is the respective total one-electron energy; a positive dissociation energy indicates the endothermic nature of the process. [d] A negative difference means the protonated case has a larger overlap population than the unprotonated one.

Table X. Summary of Various Calculated Parameters in the Analysis of $[C_5H_5Fe(CO)_2(E'H_3)]^+$ Complexes (E′ = N to Bi)[a]

	overlap populations for Fe–E′			
E′	filled levels	empty, low-lying, most antibonding orbital[a]	diff[b] $\lvert OP_{filled}\rvert - \lvert OP_{empty}\rvert$	dissocn energy,[c] eV
N	0.349	−0.025 (LUMO)	0.324	1.06
P	0.490	−0.021 (LUMO)	0.469	0.70
As	0.496	−0.036 (LUMO)	0.460	2.14
Sb	0.484	−0.036 (LUMO)	0.448	2.24
Bi	0.383	−0.019 (LUMO)	0.364	4.81

[a] Overlap populations for normally unoccupied orbitals were computed by filling them with two electrons each. [b] The difference is taken between the absolute values of the two Fe–E′ overlap populations. [c] Dissociation energy $= -[E_{complex} - E_{fragments}] = -[E_{complex} - (E_{CpFe(CO)_2^+} + E_{E'(element)H_3}]$, E is the respective total one-electron energy; a positive dissociation energy indicates the endothermic nature of the process.

indicated in the Experimental Section, yields the structures I depicted in Figures 1 (Ia–c) and 2 (Id) for the methyl- and phenyl-substituted complexes, respectively. In these structures, the iron atom adopts a pseudooctahedral coordination ("three-legged piano-stool" geometry) with two terminal carbonyl groups, one ER_2 ligand, and the cyclopentadienyl ring, which occupies the remaining three coordination sites. The overall geometry of the $[C_5H_5Fe(CO)_2]^+$ fragments is unexceptional, and the dimensions are similar to those in related $[C_5H_5Fe(CO)_2(L)]^+$ complexes.[23] No close contacts exist between the $[C_5H_5Fe(CO)_2(ER_2)]^+$ cations and the BF_4^- anions. The Fe–E bond distances (compare Tables VI and VII) are 2.264 (2) [E = S (Ia)], 2.381 (1) [E = Se (Ib)], and 2.533 (1) Å [E = Te (Ic)], slightly shorter than the respective sum of the atomic radii (2.276, 2.401, and 2.673 Å).[24] For E = S and Se, these distances are well within the range of Fe–S bond lengths in cationic $[C_5H_5Fe(CO)_2(L)]^+$ complexes (2.109 (2)–2.289 (1) Å)[25] or close to the related distances in $\{[C_5H_5Fe(CO)_2]_3Se\}^+$ (2.426–2.431 (5) Å).[26] To the best of our knowledge, no data are available for the Fe–Te bond length in cationic mononuclear iron compounds but the M–Te distance is known to depend strongly on the nature of the tellurium ligand.[27] A comparison of the Fe–S bond length for complexes Ia (R = CH_3) and Id (R = C_6H_5) shows an elongation by 0.019 Å, which is possibly due to the sterically more demanding substituents on sulfur in Id, although this value may not be statistically significant, especially in view of the limited quality of structure Id. All coordinated ER_2 ligands are oriented anti with respect to the cyclopentadienyl group, presumably to minimize steric contacts. The geometries of the coordinated $E(CH_3)_2$ ligands show

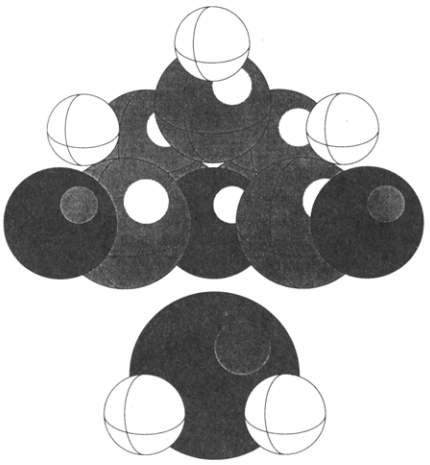

Figure 3. Space-filling drawing of the $[C_5H_5Fe(CO)_2(SeH_2)]^+$ model complex, showing an opening in the coordination sphere around the iron in between the two CO ligands.

the same overall trend as observed[28] and discussed[29] for the uncoordinated ligands: the E–C bond lengths are slightly elongated, while the C–E–C bond angles are increased by ca. 10° upon coordination of the $[C_5H_5Fe(CO)_2]^+$ fragment. A detailed discussion of the molecular structure of complex Id, except for the Fe–S bond distance, is not warranted given the limited quality of the structure.

For the theoretical calculations, geometrical parameters derived from X-ray structure determinations were used while R was taken as hydrogen. No attempts were made to explain the shortening of the Fe–E bond with respect to the sum of atomic radii.

(B) Theoretical Results. In molecular orbital calculations, the quantity that behaves as the bond strength between two atoms is the *overlap population*: the Mulliken overlap population between two atomic orbitals located on two atoms A and B in a molecule is $2c_ic_jS_{ij}$ for one electron. This corresponds to the amount of electron density transferred to the region between A and B upon interaction of the two atomic orbitals under consideration. For the overlap population between two *atoms* A and B we have to sum over the occupied [n_i = 2 (or 1) electrons] *molecular orbitals*: $OP(A-B)_{filled} = \sum 2n_{i\alpha}c_{i\alpha}c_{j\alpha}S_{ij}$. Depending on the signs of the orbital coefficients c_i, c_j, the overlap population, representing the shared electron density of A + B, can be positive or negative. From much experience, a larger positive overlap population correlates with a stronger bond and a larger bond order between A and B.[30]

(23) (a) L = CO: Gress, M. E.; Jacobson, R. A. *Inorg. Chem.* **1973**, *12*, 1746. (b) L = CS: Richardson, J. W., Jr.; Angelici, R. J.; Jacobson, R. A. *Inorg. Chem.* **1987**, *26*, 452.

(24) Calculated from data in: Fluck; Heumann. *Periodensystem der Elemente*; VCH Verlagsgesellschaft: Weinheim, FRG, 1985.

(25) (a) L = SO_2: Hartmann, G.; Froböse, R.; Mews, R.; Sheldrick, G. M. *Z. Naturforsch.* **1982**, *37B*, 1234. (b) L = dibenzothiophene: Goodrich, J. D.; Nicklas, P. N.; Selegue, J. P. *Inorg. Chem.* **1987**, *26*, 3426.

(26) Fenske, D.; Maue, P.; Merzweiler, K. *Z. Naturforsch.* **1987**, *42B*, 928.

(27) Gysling, H. J. Ligand properties of organic selenium and tellurium compounds. In *The Chemistry of Organic Selenium and Tellurium Compounds*; Patai, S., Rappoport, Z., Eds.; Wiley and Sons: Chichester, U.K., 1986; Vol. 1, p 679.

(28) (a) E = S: Pierce, L.; Hayashi, M. *J. Chem. Phys.* **1961**, *35*, 479. Iijima, T.; Tsuchiya, S.; Kimura, M. *Bull. Chem. Soc. Jpn.* **1977**, *50*, 2564. (b) E = Se: Beecher, J. F. *J. Mol. Spectrosc.* **1966**, *21*, 414. Pandey, G. K.; Dreizler, H. *Z. Naturforsch.* **1977**, *32A*, 482. (c) E = Te: Blom, R.; Haaland, A.; Seip, R. *Acta Chem. Scand.* **1983**, *A37*, 595.

(29) (a) Poirier, R. A.; Csizmadia, I. G. General and theoretical aspects of organic compounds containing selenium and tellurium. In *The Chemistry of Organic Selenium and Tellurium Compounds*; Patai, S., Rappoport, Z., Eds.; Wiley and Sons: Chichester, U.K., 1986; Vol. 1, p 21. Hargittai, I.; Rozsondai, B. Structural chemistry of organic compounds containing selenium or tellurium. *Ibid.*, p 63.

Table XI. Fe–C(Carbonyl) Overlap Populations in $[C_5H_5Fe(CO)_2(EH_2)]^+$ Complexes

		overlap populations for Fe–C (Fe–E)[a]					
		low-lying, unoccupied orbitals					
E	filled levels	OP_{LUMO}	OP_{LUMO+1}	OP_{+2}	OP_{+3}	OP_{+4}	OP_{+5}
O	0.771	0.001 (−0.184)	0.036 (0.001)	−0.070 (−0.000)	−0.160 (−0.001)	−0.074 (0.006)	−0.076 (−0.003)
S	0.766	−0.009 (−0.113)	0.038 (0.001)	−0.161 (−0.001)	−0.080 (−0.063)	−0.073 (0.004)	−0.077 (−0.000)
Se	0.765	−0.009 (−0.112)	0.038 (0.001)	−0.163 (−0.002)	−0.080 (−0.059)	−0.075 (0.002)	−0.077 (0.001)
Te	0.764	−0.018 (−0.077)	−0.038 (0.001)	−0.163 (−0.002)	−0.078 (−0.001)	−0.076 (−0.071)	−0.076 (0.004)

[a] Overlap populations (OP) for normally unoccupied levels were computed by filling them with two electrons each. The Fe–E overlap populations for these orbitals are included for comparison in parentheses to show that the Fe–C antibonding orbitals are Fe–E nonbonding.

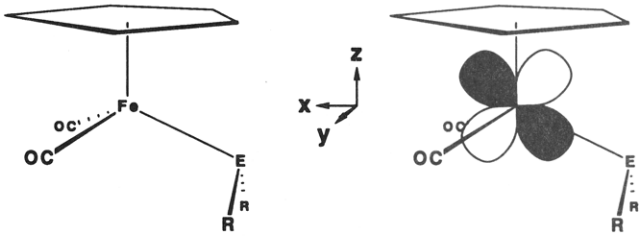

Figure 4. Schematic drawing of the model cations $[C_5H_5Fe(CO)_2(ER_2)]^+$ with the applied coordinate system used for the theoretical calculations.

The overlap populations for the Fe–E bond in the cationic complexes I are given in Table IX (first column). We see that the overlap population for E = S, Se, and Te seems about equal, while it is much smaller for E = O. There is just one dilemma: actual numbers can only be compared within a related series, keeping the atom pair A, B constant. The orbital overlap (S_{ij}) term in the definition of the overlap population is different for different orbitals or atom pairs. A way out and also more appropriate for our purpose may be to look at the difference in Fe–E overlap populations in the ground-state molecule and an energetically low-lying, *unoccupied* strongly Fe–E antibonding level. This is summarized in Table IX as well (columns 2 and 3). But why do we want to do this?

If we assume that the substitution of the ER_2 ligand proceeds predominantly via an associative or S_N2 mechanism, the nucleophilic entering group would have to interact first with a low-lying unoccupied orbital. If at the same time such an orbital has antibonding Fe–E character, then its partial filling would weaken (and lengthen) the Fe–E bond. To put this in other words, it is useful to adopt a frontier orbital perspective for bond activation. A low-lying unfilled orbital that is sterically well accessible for the incoming nucleophile is one that has an Fe orbital lobe bisecting the angle formed by the two CO ligands.

The space-filling model in Figure 3 shows an opening in the Fe coordination sphere along this line. In the coordinate system specified in Figure 4, this level would contain the d_{xz} orbital on iron. But as can be seen, one lobe of the d_{xz} set also lies along the Fe–E bond. Therefore, as the orbital interaction diagram in Figure 5 together with the values in Table IX (column 2) illustrates, this combination is of strongly Fe–E antibonding character. Figure 5 sketches the bonding and antibonding orbital interactions between the SeH_2 (as an example for EH_2) and the $[C_5H_5Fe(CO)_2]^+$ fragments and also shows the orbitals of the metal d block. The Fe(d_{xz})–E antibonding combination turns out to be the LUMO throughout our series. If we think of the cyclopentadienyl ring as occupying three coordination sites, then the $[C_5H_5Fe(CO)_2(EH_2)]^+$ cations are distorted octahedral structures. We point out in Figure 5 as well in Figure 8 the orbital sets that are reminiscent of the octahedral t_{2g}–e_g splitting. One should not get confused by the facts that the $d_{x^2-y^2}$ and d_{z^2} orbitals are part of the "t_{2g}" set. This is due to our choice of coordinate axes, where the ligands lie more along the lines between the axes, so that d_{xz} and d_{yz} are now the orbitals that experience the strongest ligand field.

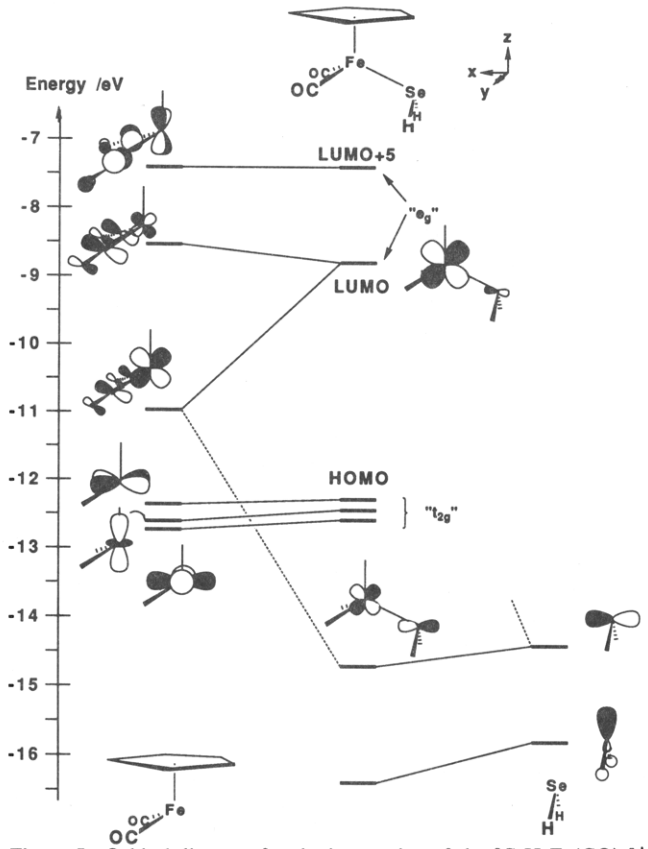

Figure 5. Orbital diagram for the interaction of the $[C_5H_5Fe(CO)_2]^+$ cation with the SeH_2 fragment. Only some orbital levels are shown and sketched schematically. The carbon C_5H_5 ring orbitals have been omitted for clarity. The combined C_{Cp} (Cp = C_5H_5) charge contributions lie between 3 and 38% for the orbitals of the full complex that are considered here.

Now, we should return to the overlap population values in Table IX: the larger the antibonding Fe–E overlap population for the unoccupied MO—necessary for the entering group—or *the smaller the respective difference* $[|OP(Fe–E)_{filled}| - |OP(Fe–E)_{empty}|]$, then the *more labile* (*less inert*) the complex i.e. more prone to substitution, should the leaving group ER_2 become. And indeed the differences follow the experimental trend, with oxygen—which is most labile—having the smallest value. Selenium has a slightly larger difference than sulfur, in agreement with equilibrium studies.[4a] Tellurium, which is the most inert in this series, has the largest value. Looking at these differences provides, however, only a very crude first approximation, since it does not take into account any rearrangement of the ligands to allow association of the nucleophile and formation of the activated complex.

The Fe–E bond dissociation energy which one might take as an indicator for the thermal stability of the Fe–E bond suggests a decrease in bond strength in the order Fe–Te > Fe–Se > Fe–S > Fe–O, coinciding with the lability trend. The values are included in Table IX (fourth column). Were the substitution reaction to proceed more via a dissociative of S_N1 mechanism, one might view

(30) (a) Albright, T. A.; Burdett, J. K.; Whangbo, M.-H. *Orbital Interactions in Chemistry*; Wiley-Interscience: New York, 1985. (b) Hoffmann, R. *Solids and Surfaces: A Chemists View of Bonding in Extended Structures*; VCH Verlagsgesellschaft: Weinheim, FRG, 1988.

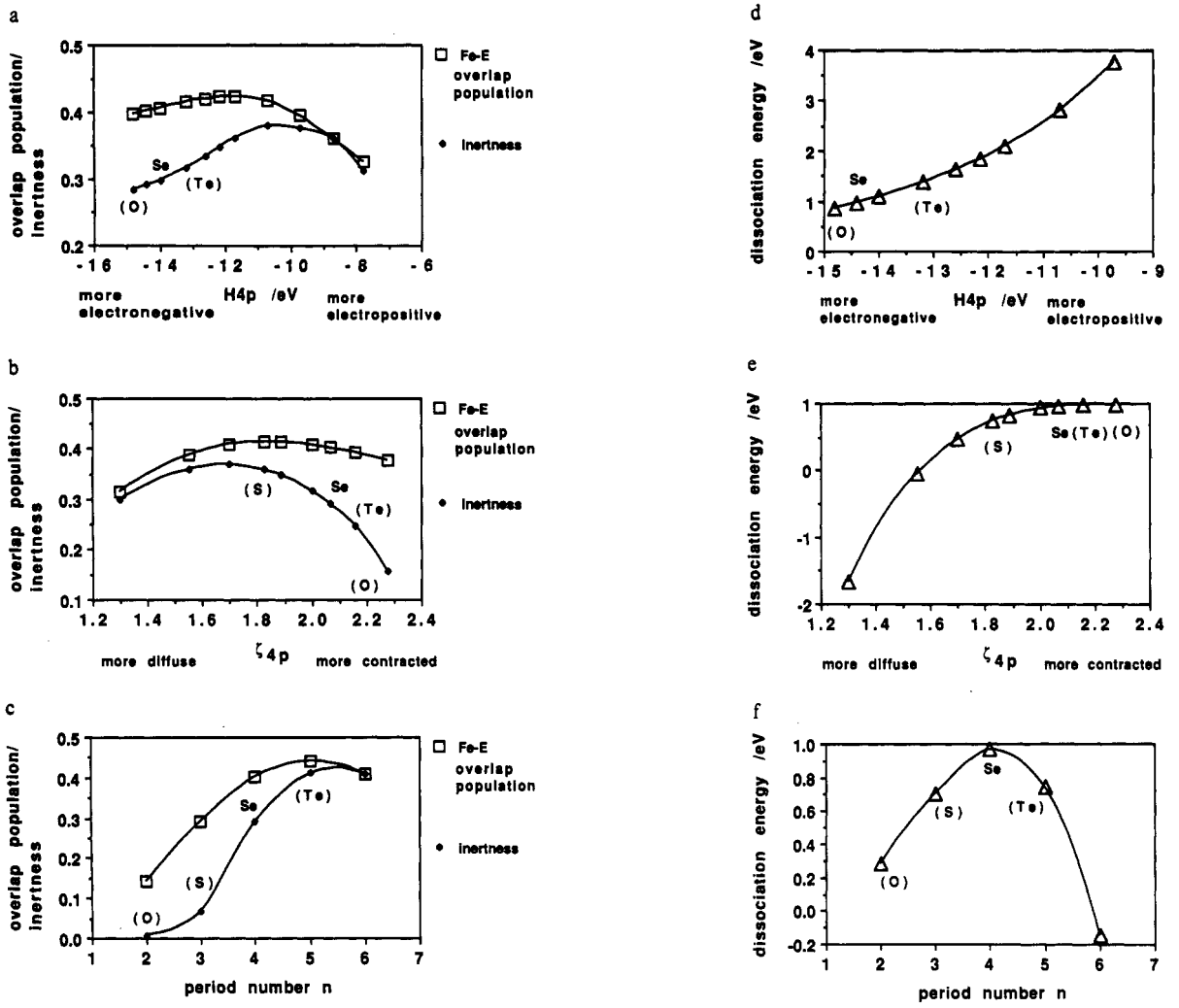

Figure 6. Graphical representations for the parameter dependency of the overlap population on the inertness (a–c) and the dissociation energy (d–f) of the Fe–E bond in $[C_5H_5Fe(CO)_2(EH_2)]^+$ complexes. The set of the Se parameters was taken as a starting point for the single-parameter variation of (a, d) the 4p orbital energy (H_{4p}), (b, e) the 4p Slater exponent (ζ_{4p}), and (c, f) the period number n. (Elemental symbols in parentheses mark their respective parameters.)

the Fe–E dissociation energy as a measure of lability for the Fe–E bond. The larger the value of the dissociation energy, the more inert would the complex be with respect to breaking of the Fe–E bond as the possible rate-limiting step in the formation of a 5-coordinate intermediate. However, one must not confuse the terms *stable/unstable* with *labile/inert*. *Inert* complexes simply have no suitable low-energy pathway for the reaction (be it S_N2, S_N1 alone, or intermediate mechanism) available, or in other words, the free energy of activation is very high even if there are more stable products. A *stable* complex has a large positive free energy of reaction for its decomposition.[31] Of course, in the absence of kinetic studies, the extended Hückel method cannot predict which mechanism (associative, dissociative, or intermediate) would be the preferred one, especially since entering group or medium effects are also important in stabilizing a 7-coordinate (S_N2) or, respectively, 5-coordinate (S_N1) intermediate, just to mention the extreme possibilities.

Table X summarizes the overlap populations of the filled levels, the $Fe(d_{xz})$–E′ antibonding LUMO, and their difference for the Fe–group 15 donor bond (E′ = N–Bi), for comparison. The difference in overlap populations as a measure for the kinetic lability suggests a displacement order of P > As > Sb > Bi > N; i.e. PR_3 should replace all other ligands in this series. On the other hand, the dissociation energy (indicator for thermal stability or S_N1 lability; also included in Table X) predicts the opposite trend (Bi > Sb > As > N > P), with Bi being most inert. Except for the reversed order observed between Bi and N, the analysis based on the overlap population difference is in agreement with the experimental results.[3] Calculating the bismuth ligand is more inert than nitrogen should not be considered a failure, however, since we did not explicitly account for possible relativistic effects[32] in the Fe–Bi bond and we had to estimate the Fe–N bond length. Steric factors may also play a dominant role in the exchange between $E'R_3$ ligands. Steric constraints are of course part of the kinetic lability/inertness of a complex but are not accounted for in our calculation with simplified ligands. A limited space for the substitution reaction around the metal center may give the smaller P and N ligands an additional advantage over their larger congeners, thereby possibly reversing the order N/Bi and leading to the very fast exchange by the $P(CH_3)_3$ ligand. Steric factors may figure more prominent for the $E'(CH_3)_3$ ligands (E′ = N–Bi) with respect to $E(CH_3)_2$ (E = O–Te) due to the additional methyl group in the former.

One could continue to ask why is the Fe–Te bond the most inert (regardless of the mechanism at work) and apparently the most stable one in the group 16 series, and why does one not see the same trend in the Fe–group 15 donor bonds?

We tried to trace these trends to some inherent properties of the donor atom E, such as electronegativity, diffuseness, and size of its lone-pair donor orbital (which is mainly p type in character;

(31) (a) Huheey, J. E. *Inorganic Chemistry*, 3rd ed.; Harper and Row: New York, 1983; p 547 ff. (b) Cotton, F. A.; Wilkinson, G. *Advanced Inorganic Chemistry*, 5th ed.; Wiley-Interscience: New York, 1988; Chapter 29.

(32) Pyykkö, P. *Chem. Rev.* **1988**, *88*, 563.

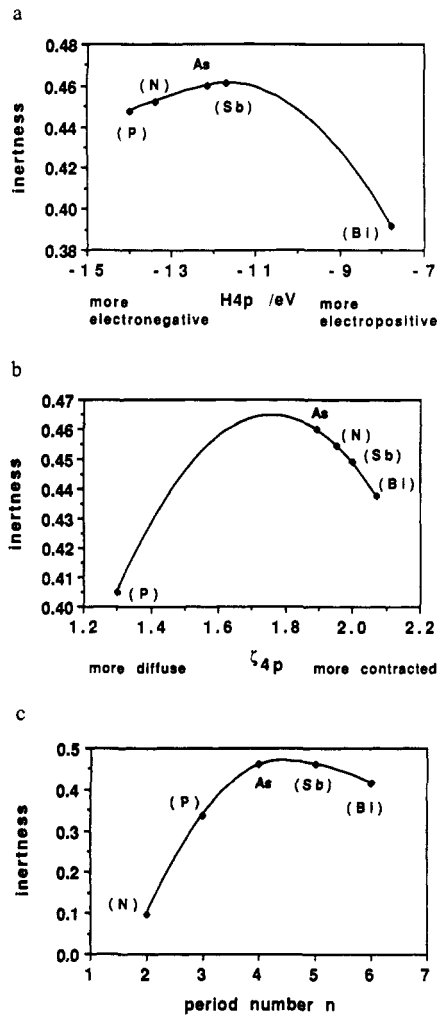

Figure 7. Graphical representation for the parameter dependency of the inertness of the Fe–E′ bond in $[C_5H_5Fe(CO)_2(E'H_3)]^+$ complexes (E′ = N–Bi). The set of As parameters was taken as a starting point for the single-parameter variation of (a) the 4p orbital energy (H_{4p}), (b) the 4p Slater exponent (ζ_{4p}), and (c) the period number n. (Elemental symbols in parentheses mark their respective parameters.)

see orbital sketches in Figure 5). These features are determined by our choice of calculational parameters: the np orbital energy correlates mainly with the electronegativity, the Slater exponent ζ_{np} with the diffuseness, and the period number n with the size of the orbital.

In order to see the consequences in the change of one particular variable, we arbitrarily chose the selenium as a donor atom and then varied one parameter at a time keeping the others constant. The resulting trends in the Fe–E overlap population, the lability, or the dissociation energy, then gave a general ideal on the parameter and subsequently electronegativity, diffuseness, and size dependency of the E donor orbital. (Of course, the elementary properties cannot really be this well separated nor attributed to just one calculational parameter as we do it here.) Parts a–f of Figure 6 picture these trends. For a discussion, we will take the Se values as a starting and reference point. The variational parameters which equal the respective ones from other members of the group have been marked by the elemental symbol in parentheses.

Figure 6a shows the overlap population/inertness (for S_N2) of the Fe–E bond as a function of the 4p orbital energy. Starting from Se, we see an increase in both values as the orbital to a higher energy and then a maximum followed by a decline. The maxima occur roughly around the orbital energy calculated for the d_{xz}-containing MO on iron (−10.95 eV; compare Figure 5), which is the main bonding partner for the E lone pair. This is expected, since the overlap population is inversely proportional to the energy difference between the two interacting orbitals on both fragments.

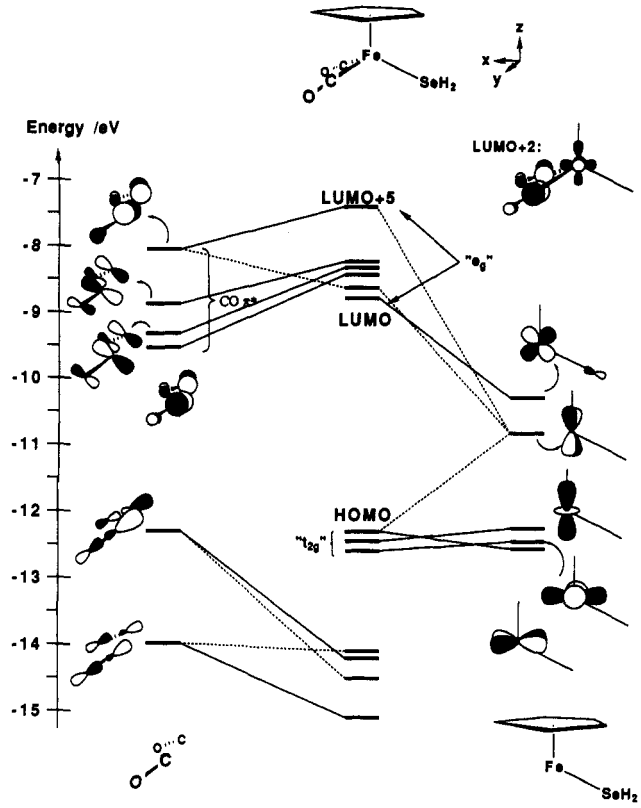

Figure 8. Orbital diagram for the interaction of the $[C_5H_5Fe(SeH_2)]^+$ cation with the $(CO)_2$ fragment. Only a few levels are shown and their orbital drawings sketched schematically. Carbon C_5H_5 orbitals are omitted for clarity. Their combined charge contributions lie between 2 and 35% for orbitals of the full complex that are shown here.

The orbital energies within the O–Te series follow the expected trend (the p orbital energy for S is slightly more negative than for Se).

For the overlap population/inertness dependency on the Slater orbital coefficient (given in Figure 6b) we also find an optimum and a decline if the orbital gets too diffuse or too contracted. The contracted oxygen lone pair shows the expected low inertness (high lability). However, when S, Se, and Te are compared, the trend is not as seen earlier. This leads us to conclude that the other parameter variables (np orbital energy, n) are apparently more important.

The variation in the size of the orbital upon changing the period number (Figure 6c, ζ_{4p} implies a smaller size variation as well, of course) shows the strongest shifts in overlap population/inertness—a large decrease toward S and O, which have the smaller orbitals, and an increase toward the larger lobes on Te.

The respective curves for the dissociation energy correlating to the thermodynamic stability are given in Figure 6d–f. When the orbital energy rises (a more electropositive atom), we see a steady increase in dissociation energy (Figure 6d), with the variation among the group 16 donors as seen earlier (Table IX). On the other hand, contracted orbitals, as for example on O, would seem to give higher dissociation energies than the more diffuse ones (Figure 6e). However, in the case of oxygen this tendency is compensated for by its small size, which again leads to a smaller dissociation energy than its heavier congeners (Figure 6f).

The curves given for the H_{np} and ζ_{np} variation represent cross sections of a surface that describes simultaneous displacements in these two parameters for $n = 4$. The variation with n then shows the distance between the surfaces for the different n at a given H_p, ζ_p set (here, the one for E = Se).

A similar single-parameter variation within the E′ complexes—taking arsenic as a reference point—does not give quite as clear a picture. The variations of the inertness (overlap population difference between the filled levels and the LUMO) as a function of the 4p orbital energy and Slater coefficient, as well as the principal quantum number n, are shown in Figure 7

parts a-c, respectively. Apparently, the lability of the bismuth ligand can be traced to its electropositive character (Figure 7a), while the one for nitrogen is due to its small orbital size (Figure 7c). To elucidate the lability/inertness ordering among P, As, and Sb from a single-parameter variation is not possible, in part because the differences in overlap population values (given in Table X) are fairly small. Also, the s orbitals or s-p hybridization may play a more important role in influencing the lability of the E' ligands. However, for both group 15 and group 16 ligand sets, the rationalization of the trend based on a single parameter variation is still only a first rough picture, since the change in Fe-E(E') bond length was not accounted for, the s orbital contributions were left aside, and it is the combination of all the parameters in the semiempirical method that really defines and characterizes an element.

We do not think, however, that the difference between the group 15 and group 16 elements is due to the second lone pair and the possibility for E to Fe π bonding by the former. To probe this assumption, we protonated the EH_2 group, thereby tying up its second lone pair in E-H bonding and making it unavailable for a potential π bond to the metal. On comparing the Fe-E overlap populations for the nonprotonated and protonated case (Table IX; compare column 1 with 6 and 7), we find only a very small difference. In the case of S, Se, and Te, the protonated EH_3^+ group even leads to a very slightly larger Fe-E overlap population than its conjugated base, indicating that if the (second) lone pair has any effect at all, that effect is antibonding. As for the increasing electron density on the iron center in the order S- < Se- < Te-complex I, which was deduced from experimental NMR data (high-field shift of C_{Cp} (Cp = C_5H_5) from S to Te and of C_{CO} from Te to S) and IR data (lower ν_{CO} from S to Te),[4a] we are able to theoretically reproduce this trend. The computed net charges on iron are included in Table IX (column 5).

We think we can also provide an understanding of the photosubstitution of a CO group, rather than the conceivable photosubstitution of an ER_2 group. The latter is not observed experimentally.[4a,4b] Figure 8 gives the orbital diagram between the two CO's and the $[C_5H_5Fe(SeH_2)]^+$ fragment. As in Figure 5, the HOMO and the orbitals directly below are mostly Fe d in character. And so is the LUMO. Hence, the lowest energy, HOMO-LUMO, absorption would correspond to a "forbidden" d-d transition ($\Delta l = 0$)—although the LUMO might still be the photoactive state. Two to six orbitals above the LUMO, still very close in energy to it, lie orbitals which are primarily the four CO π^* levels, but which also contain an Fe-CO antibonding component. The Fe-C_{CO} overlap populations for these normally unfilled levels are listed in Table XI. These CO π^* orbitals can give rise to metal-ligand charge-transfer processes, involving the formal oxidation of Fe^{2+} to Fe^{3+}. Promoting electrons to these Fe-CO antibonding orbitals upon irradiation then leads to more labile carbonyl ligands, leaving, however, the Fe-ER_2 group bonding untouched (the Fe-E overlap populations are included in parentheses in Table XI). We note that the Fe-C_{CO} bond strengths as given by the overlap populations are rather similar for all complexes with E = O-Te (see values in Table XI).

Acknowledgment. H.S. is indebted to Profs. Dr. R. W. Parry and T. G. Richmond (University of Utah) for their support and interest in this work during his stay at the University of Utah (1987/1988) and to the Studienstiftung Des Deutschen Volkes, Bonn, FRG, for a stipend. R.H. and C. J. thank the Deutscher Akademischer Austauschdienst (DAAD) for the award of a NATO postdoctoral fellowship for C.J. and the National Science Foundation for its generous support through Grant CHE-89-12070.

Supplementary Material Available: Structural figures of Ia-d and listings of thermal and positional parameters, complete bond distances and angles, least-squares planes, and crystal data (30 pages); tables of calculated and observed structure factors for complexes Ia-d (45 pages). Ordering information is given on any current masthead page.

Contribution from the Corporate Research Science Laboratories, Exxon Research and Engineering Company, Annandale, New Jersey 08801, and the Department of Chemistry, Massachusetts Institute of Technology, Cambridge, Massachusetts 02139

Magnetostructural Correlations in Magnetically Coupled (μ-Oxo)diiron(III) Complexes

Sergiu M. Gorun*,[1a] and Stephen J. Lippard*,[1b]

Received November 27, 1990

A quantitative magnetostructural relationship has been found for dinuclear iron(III) centers bridged by a ligand oxygen atom (oxo, hydroxo, alkoxo, etc.) and at least one other bridging ligand (carboxylate, sulfate, phosphate, etc.). A correlation exists between the antiferromagnetic exchange-coupling constant J (in cm^{-1}) and P, a parameter having units of distance (in Å) defined as half the shortest superexchange pathway between two iron(III) ions. Specifically, $-J = A \exp(BP)$ where $A = 8.763 \times 10^{11}$ and $B = -12.663$. Results for 36 dinuclear metal centers, including Fe_2 and Fe_3, complexes have been used to derive this relationship, which can also be applied to tetranuclear complexes and metalloproteins. This magnetostructural correlation is shown to have powerful predictive properties, although it does not apply to (μ-oxo)diiron(III) centers unsupported by other bridging ligands. Attempts to correlate J with any other structural parameters such as the Fe-O-Fe angle or Fe···Fe distance for ligand-bridged $[Fe_2O]^{4+}$ cores were unsuccessful.

It has long been recognized that for open-shell, ligand-bridged polymetallic compounds, some correlation must exist between the type and magnitude of magnetic interactions and the relative positions of the metal ions.[2] Magnetic studies on copper acetate[3] and basic metal carboxylates[4] revealed antiferromagnetic interactions, from which their respective dinuclear and trinuclear structures[5] were correctly predicted. A major thrust of numerous subsequent papers has been to establish quantitative correlations between structural and magnetic properties. This interest stems in part from the desire to understand at a fundamental level what determines the size and magnitude of exchange-coupling inter-

(1) (a) Exxon Research and Engineering Co. (b) Massachusetts Institute of Technology.
(2) (a) Néel, L. *Compt. Rend.* **1936**, *203*, 304 and references therein. (b) Goodenough, J. B. *Phys. Rev.* **1955**, *100*, 564. (c) Goodenough, J. B. *Phys. Chem. Solids* **1958**, *6*, 287. (d) Kanamori, J. *Phys. Chem. Solids* **1959**, *10*, 87.
(3) Bleaney, B.; Bowers, K. D. *Proc. R. Soc. London* **1952**, *A214*, 451.
(4) Kambe, K. *J. Phys. Soc. Jpn.* **1950**, *5*, 48.
(5) (a) Van Niekerk, J. N.; Schoening, F. K. L. *Acta Crystallogr.* **1953**, *6*, 227. (b) Figgis, B. N.; Robertson, B. G. *Nature* **1965**, *205*, 694.

0020-1669/91/1330-1625$02.50/0